Role of Mg on Mn-Bearing Dispersoids and Their Impact on Mechanical Properties and Recrystallization Resistance of Cold-Rolled 5xxx Alloys

Ahmed Y. Algendy, Kun Liu, and X. -Grant Chen

Abstract

The evolution of the Mn-bearing dispersoids in two Al-Mg-Mn 5xxx alloys with 3% and 5% Mg and their impact on the mechanical properties and recrystallization resistance have been investigated. A large number of Mn-dispersoids were precipitated in the aluminum matrix by applying a low-temperature homogenization, but the type, size, and number density of these dispersoids after heat treatment were strongly related to the Mg levels: fine Al_6Mn and α-Al(Mn,Fe)Si dispersoids were observed in Al-3 Mg-Mn alloy, while the dispersoids changed to relatively large Al_4Mn and Al_6Mn dispersoids in Al-5 Mg-Mn alloy. The mechanical properties after cold rolling as a function of the annealing temperature were studied. The yield strength after cold rolling and 300 °C annealing reached 233 MPa for low Mg and 253 MPa for high Mg alloys homogenized at low temperature, respectively, showing an improvement of 30% and 20% over the high-temperature homogenization. In addition, the deformed grain structures after cold rolling and annealing were characterized. Results demonstrated that fine and densely distributed Mn-dispersoids generated during low-temperature homogenization could effectively hinder the dislocation and sub-grain boundary migration and improve the recrystallization resistance of cold-rolled sheets.

Keywords

AA5xxx Alloys · Mn-dispersoids · Cold rolling · Mechanical properties · Recrystallization resistance

1 Introduction

Al-Mg-Mn 5xxx alloys are popular for their lightweight, excellent toughness, and corrosion resistance, making them suitable for a broad range of applications in transportation, structural, and chemical industries [1, 2]. However, their strength is limited as non-heat-treatable alloys due to lack of precipitation strengthening [3]. Increasing the magnesium content can improve strength but may cause the reduction of the ductility and corrosion resistance. Commercial 5xxx alloys contain 3–6% Mg [1, 4]. Recent studies have shown that Mn-bearing dispersoids, formed through appropriate heat treatments, can enhance the room and elevated temperature properties of non-heat-treatable aluminum alloys, providing supplemental strength and preserving deformed structures during post-deformation annealing [5–7].

Many commercial Al-Mg-Mn 5xxx alloys, such as AA5083, AA5454, AA5754, and AA5182, contain high Mn level and small amounts of Fe and Si impurities. These impurities result in the formation of either coarse intermetallic phases during solidification or fine dispersoids during homogenization. It is reported that changing the Mg levels affects the formation of Fe/Mn-containing intermetallic compounds [8, 9]. Mn-bearing dispersoids, such as $Al_6(Mn,Fe)$, $Al_m(Mn,Fe)$, α-Al(Mn,Fe)Si, and ε-$Al_{18}(Mn,Cr)_2Mg_3$ are the common precipitates in AA5xxx alloys during homogenization [4, 5, 10–12]. However, the alloy composition and homogenization parameter can greatly influence the formation of these dispersoids [4, 5, 10]. Engler

A. Y. Algendy (✉) · K. Liu · X. -G. Chen
Department of Applied Science, University of Quebec at Chicoutimi, QC, Canada
e-mail: aalgendy@etu.uqac.ca

Proceedings of the 62nd Conference of Metallurgists, COM 2023, https://doi.org/10.1007/978-3-031-38141-6_31

et al. [4, 10] reported that both α-Al(Mn,Fe)Si and Al_6(Mn,Fe) dispersoids precipitated during homogenization in several Al-Mg-Mn alloys, depending on the Si and Mg content. In addition, a low-temperature heat treatment can produce finer and more uniformly distributed dispersoids than a high-temperature treatment, which provides an extra strengthening effect [5, 13].

Al-Mg-Mn 5xxx alloys are usually delivered in sheet form for various transportation and structural applications. After homogenization, the cast ingots undergo hot and cold rolling to produce the final sheet products. Dynamic recovery and recrystallization during hot rolling control the formability and work hardening, and the retardation of recrystallization can improve the mechanical properties [14]. For thin sheets, cold rolling is often applied. However, cold rolling introduces defects and increases the stored deformation energy, but subsequent annealing stabilizes the microstructure through the static recovery and recrystallization process, improving the ductility and reducing work hardening. The degree of recrystallization is affected by the annealing temperature and time, as well as the volume fraction and size of dispersoids formed during homogenization. Controlling the size and distribution of Mn-bearing dispersoids can, therefore, significantly improve the materials performance [10, 13].

Although Mg is not an essential dispersoid-forming element, the present study was undertaken to understand the role of Mg in forming the Mn-dispersoids and their influence on the alloy properties of the final product in two cold-rolled Al-Mg alloys. The results were compared with a traditional homogenization treatment. The microstructure evolution during heat treatment, hot and cold rolling, was characterized using optical microscopy (OM), scanning electron microscopy (SEM), electron backscatter diffraction (EBSD), and transmission electron microscopy (TEM).

2 Experimental Procedure

Two Al-Mg-Mn alloys with two Mg levels, denoted as L-Mg and H-Mg alloys, were prepared by conventional melting and casting procedures. The designed chemical compositions of L-Mg and H-Mg are close to the chemical specification of AA5454 (Al3MgMn) and AA5083 (Al4.5MgMn) alloys. Table 1 lists the actual chemical composition of two alloys studied. After preparing the molten metal by melting the master alloys with a desirable composition, the melt was cast into a permanent steel mold preheated at 250 °C to produce the cast ingots with a dimension of 30 × 40 × 80 mm.

The cast ingots were heat-treated with a low-temperature three-step homogenization (275 °C/12 h + 375 °C/48 h + 425 °C/12 h) to promote the precipitation of Mn-bearing dispersoids and adapt the hot rolling process [7]. In addition, few ingots were subjected to an industrial high-temperature homogenization (430 °C/2 h + 480 °C/2 h + 525 °C/2 h) as the control base [7]. The homogenized ingots were hot-rolled at 500 °C to produce a flat plate with an 88% reduction. The hot-rolled plates with a thickness of 3.2 mm were further cold-rolled to a final thickness of 1 mm with a 69% reduction. The cold-rolled samples were annealed at 200–400 °C, followed by air cooling.

Uniaxial tensile testing was performed at room temperature using an Instron 8801 servo-hydraulic unit with a strain rate of 0.001 S^{-1}. The tensile samples were machined according to ASTM E8/E8M-16a in the rolling direction. Average results were obtained from three repeated tests.

The microstructures were observed under optical microscopy (Nikon, Eclipse ME600), scanning electron microscope (SEM, JEOL-JSM-6480LV), and transmission electron microscope (TEM, JEM-2100). In addition, the annealed samples were sectioned in the rolling direction and observed with electron backscattered diffraction (EBSD) technique with scan step sizes of 1 μm. TEM thin foils were prepared in a twin-jet electro-polisher using a solution of 30% nitric acid in methanol at − 20 °C to study the characteristics of Mn-bearing dispersoids. The size and number density of Mn-bearing dispersoids were measured using ImageJ analysis software on TEM images. The number density and the volume fraction of Mn-bearing dispersoids were measured according to the method described in [7].

Table 1 Chemical composition of the experimental alloys (wt.%)

	Mg	Mn	Si	Fe	Cu	Cr	Ti	Al
L-Mg	**3.01**	0.81	0.27	0.31	0.10	0.14	0.09	Bal.
H-Mg	**4.78**	0.79	0.26	0.31	0.10	0.15	0.10	Bal.

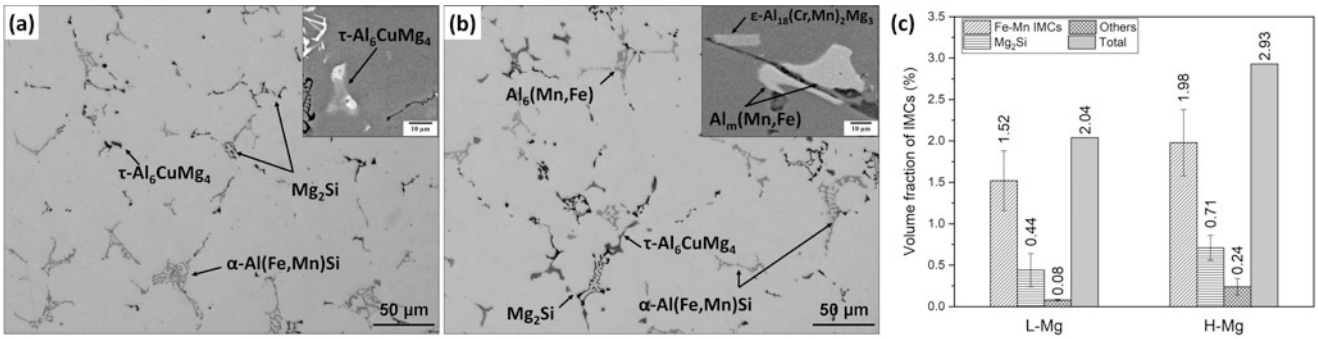

Fig. 1 Optical micrographs and inserted SEM images showing the distribution of intermetallic phases of the experimental alloys in as-cast condition (**a**) L-Mg alloy, (**b**) H-Mg alloy, and (**c**) the volume fractions of IMCs phases in both alloys

3 Results and Discussion

3.1 Microstructure Evolution in the As-Cast and Homogenized Samples

Figure 1 shows optical micrographs with inserted SEM images revealing the distribution of various intermetallic phases (IMCs) in as-cast L-Mg and H-Mg alloys. In addition, the volume fraction of various IMCs is summarized in Fig. 1c. As shown in Fig. 1a, b, the as-cast structure was composed of α-Al dendrite cells as the matrix and complex-shaped intermetallic particles with various morphologies and contrast located in the interdendritic regions. Alloy L-Mg (Fig. 1a) revealed the presence of three intermetallic phases: α-$Al_{15}(Fe,Mn)_3Si_2$ (irregular and bright phases with high Si content), Mg_2Si (dark phase), and a minor fraction of the low melting-point eutectic phase of τ-Al_6CuMg_4. Alloy H-Mg (Fig. 1b) displayed a large number of IMC phases, including $Al_6(Mn,Fe)/Al_m(Mn,Fe)$ without Si, a minor fraction of α-$Al_{15}(Fe,Mn)_3Si_2$ and ε-$Al_{18}(Cr,Mn)_2Mg_3$, Mg_2Si, and the low eutectic melting phase τ-Al_6CuMg_4 [8]. In addition, the volume fraction of IMCs increased with increasing Mg content (2.04% in L-Mg vs. 2.93% in H-Mg). It can be seen that increasing the Mg content not only alters the type of IMCs phases but also increases their volume fraction. However, changing the type of IMCs by increasing the Mg content may be attributed to two reasons: (1) lowering the peritectic temperature during solidification [9] and (2) lowering the Si/Mg ratio [8], where higher Si/Mg ratio stabilizes the formation of α-$Al_{15}(Fe,Mn)_3Si_2$ (in L-Mg) over $Al_6(Mn,Fe)/Al_m(Mn,Fe)$ (in H-Mg) [15, 16].

The microstructures of both alloys after the low-temperature homogenization are presented in Fig. 2. It can be seen that a large number of submicron dispersoids were precipitated in the dendrite cell interiors. Figure 2a, b shows the distribution of the dispersoid zones (DZs) and the dispersoids free zones (DFZs) in both alloys. The precipitation of dispersoids in the DZs was further studied in detail using TEM (Fig. 2c, d). The chemical compositions of dispersoids, measured by STEM-EDS point analysis, are listed in Table 2. As shown in Fig. 2c, L-Mg alloy contained two kinds of dispersoids with different morphologies; one was the small round-shaped particles and another was rod-shaped particles. STEM-EDS analysis of the round-shaped particles revealed high Mn, Fe, and Si contents, and thus, the round-shaped particles were presumably classified as α-Al(Fe,Mn)Si. The rod-like particles held high Mn and Fe but without Si, and was identified as $Al_6(Mn,Fe)$. On the other hand, H-Mg alloy also exhibited two different Mn-dispersoids with different aspect ratios (Fig. 2d). The STEM-EDS analysis confirmed that both types of dispersoids contained Mn and Fe but without Si. The rod-like particles were identified as $Al_6(Mn,Fe)$, while the dispersoids with cube-like morphology were classified as $Al_4(Mn,Fe)$ according to Mn/Fe ratio. Those three types of dispersoids were frequently observed in homogenized 5xxx series alloys [5, 11].

The characteristics of Mn-dispersoids were quantified from the TEM images, and the results are presented in Table 3. Regarding different dispersoids, all types of dispersoids are designated as Mn-bearing dispersoid in the following text since they have a similar influence on the mechanical properties and recrystallization. The size of dispersoids in H-Mg alloy was larger than that in L-Mg alloy (24.8 nm vs. 19 nm). On the other hand, the number density of dispersoids remarkably decreased by increasing Mg content. For example, the density of dispersoids decreased from 799×10^{19} m^{-3} (L-Mg) to 560×10^{19} m^{-3} (H-Mg). It can also be found that the volume fraction of DFZs increased by increasing the Mg content (21.3% in L-Mg vs. 27.4% in H-Mg). It is well known that DFZs located in the interdendritic regions and originated from the periphery of Mn-rich intermetallic phases due to Mn depletion nearby these phases [6]. Therefore, compared to L-Mg alloy, H-Mg alloy exhibited a larger volume fraction of the Mn-Fe IMC phases (Fig. 1c), resulting in a higher volume fraction of DFZs.

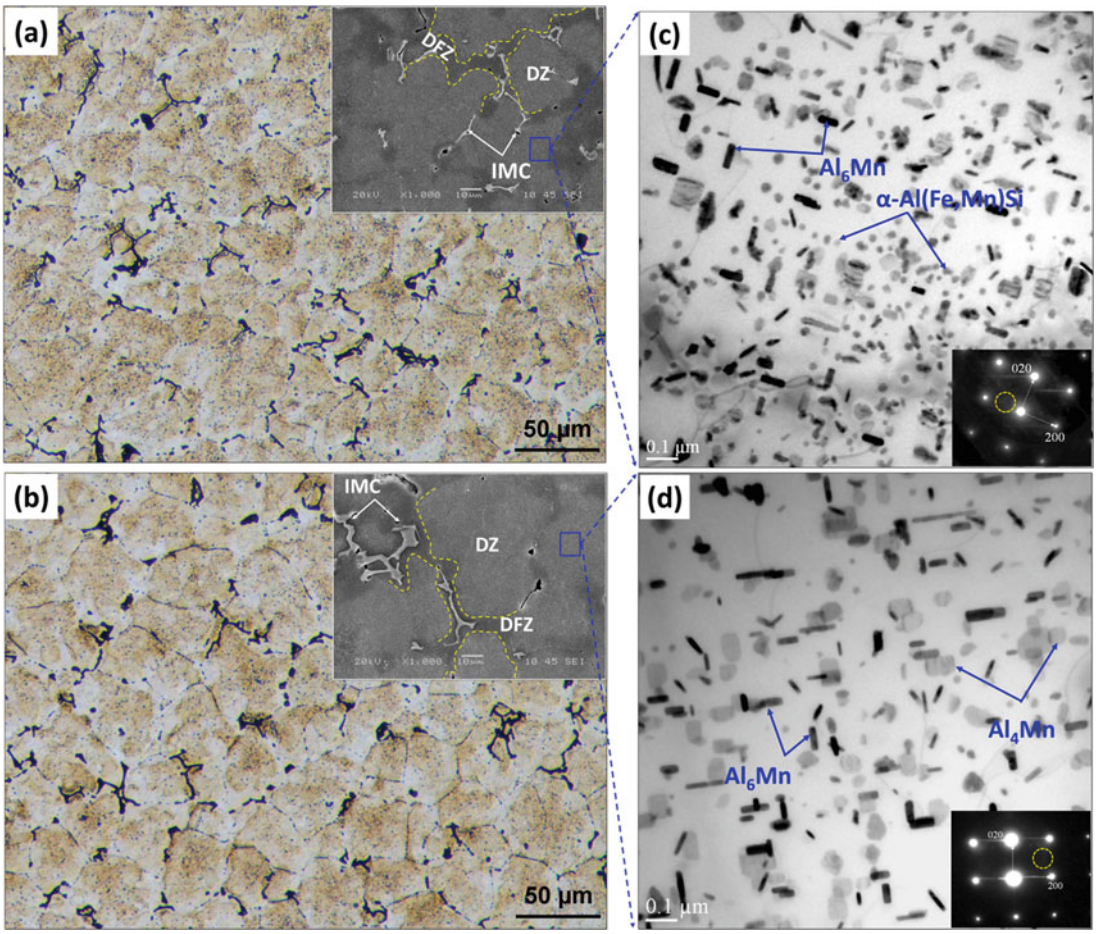

Fig. 2 The optical micrographs with inserted SEM images for (**a**) L-Mg and (**b**) H-Mg alloys, showing the distribution of DZs and DFZs after the low-temperature homogenization. Bright-field TEM images of (**c**) L-Mg and (**d**) H-Mg alloys, showing the type and distribution of dispersoids in DZs

Table 2 Statistical results of TEM-EDS analysis (at.%) of different Mn-dispersoids

		Mg	Mn	Fe	Si	Cr	Al
L-Mg	α-Al(Fe,Mn)Si	2.90 ± 0.5	2.88 ± 0.4	0.29 ± 0.6	0.99 ± 0.7	0.42 ± 0.9	Bal.
	Al_6Mn	2.81 ± 0.6	2.95 ± 0.3	0.31 ± 0.4	–	0.47 ± 0.4	Bal.
H-Mg	Al_4Mn	4.21 ± 0.3	7.90 ± 0.4	0.72 ± 0.2	–	0.94 ± 0.3	Bal.
	Al_6Mn	4.32 ± 0.2	2.31 ± 0.1	0.21 ± 0.3	–	0.50 ± 0.2	Bal.

3.2 Mechanical Properties and Recrystallization Resistance

Figure 3 presents the mechanical properties of the cold-rolled and annealed sheets of experimental alloys as a function of the annealing temperature. In addition, an industrial high-temperature homogenization before rolling was applied as the control base to understand the role of Mn-bearing dispersoids on the mechanical properties. Figure 3a, c displays the typical engineering stress-strain curves for L-Mg and H-Mg alloys. In general, after reaching the peak stress (ultimate tensile strength), the stress-strain curve underwent a short plateau followed by an instantaneous drop. The yield strengths (YS) of H-Mg alloy were always higher than those of the L-Mg alloy, mainly attributed to the higher Mg solid solution strengthening [3]. Furthermore, the YS significantly increased from after hot rolling to after cold rolling due to the strong strain hardening effect (198 MPa vs. 366 MPa in L-Mg and 230 MPa vs. 382 MPa in H-Mg), while the elongation decreased by 4–5.6%. It can be also seen that the YS after the low-temperature homogenization (LTH, solid lines) were always higher than those after the industrial high-temperature homogenization (HTH, dash lines), primarily due to the higher number density of dispersoids generated by the LTH.

Table 3 Characteristics of Mn-bearing dispersoids and DFZ after heat-treated

	Equivalent diameter $\overline{D}$, nm	Number density Nd, $\times 10^{-19}$, m^{-3}	DFZ%
L-Mg	19.1 ± 1.5	798.9 ± 53.9	21.3 ± 2.1
H-Mg	24.8 ± 1.7	559.8 ± 22.2	27.3 ± 3.2

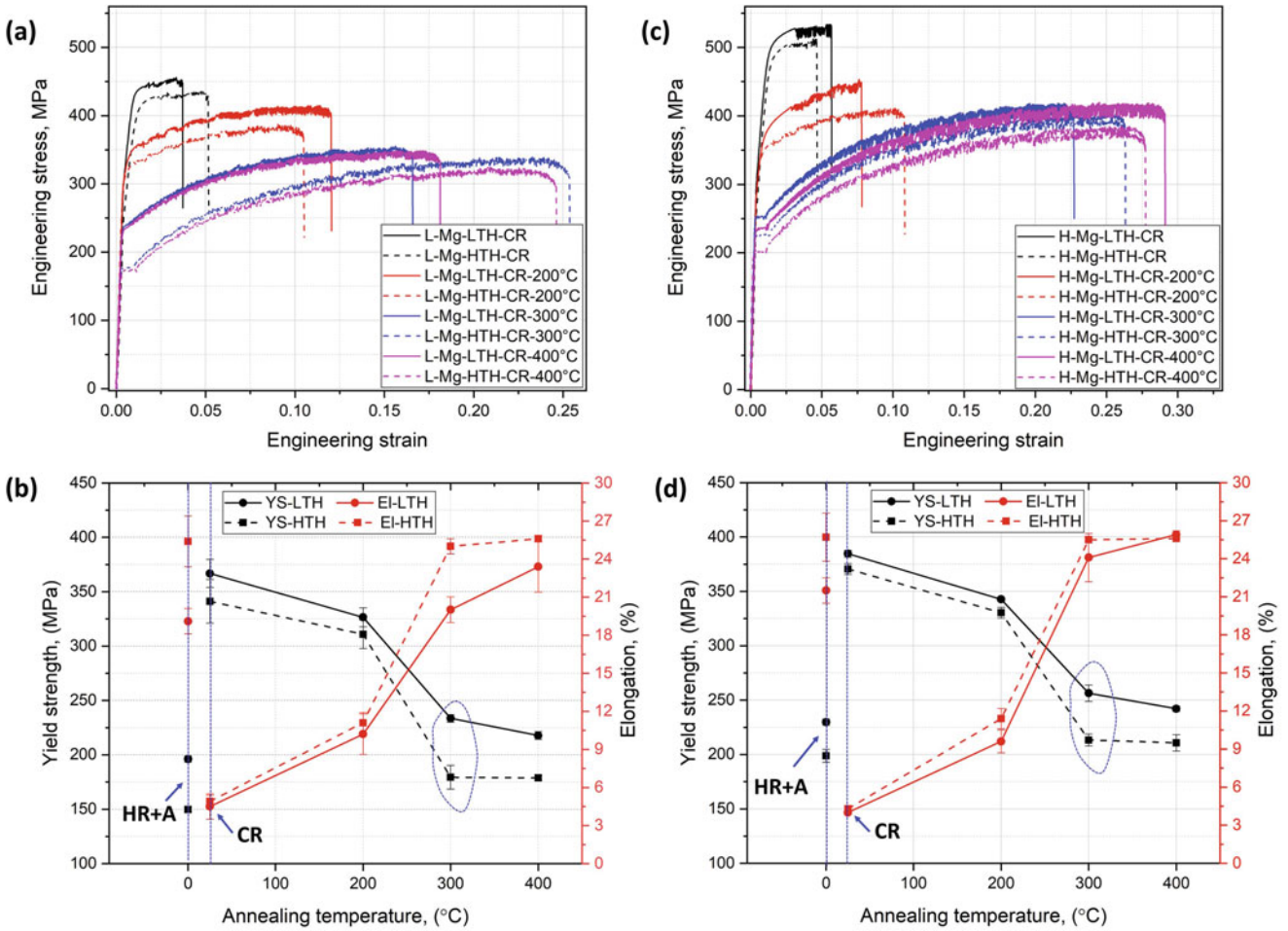

Fig. 3 (**a**) Typical engineering stress-strain curves; (**b**) yield strength and elongation as a function of the annealing temperature of L-Mg alloy; (**c**) typical engineering stress-strain curves; and (**d**) yield strength and elongation as a function of the annealing temperature of H-Mg alloy. HR-A refers to the hot rolling plus 300 °C/5 h annealing, and CR refers to the cold rolling

During post-annealing, the trend of the mechanical strength changes in both alloys was similar. The YS decreased as the annealing temperature increased, while the elongation increased due to the static recovery and recrystallization. As shown in Fig. 3b, d, the YS gradually decreased at a relatively low annealing temperature (200 °C), while there was a sharp decrease at 300°C followed by a plateau until 400 °C because of the change of deformed grain structure during annealing [17, 18]. At low annealing temperature (i.e., 200 °C), both samples remained in the recovery stage, and the small difference in the YS between two homogenization conditions (~25 MPa in L-Mg and ~ 12.4 MPa in H-Mg) was mainly attributed to the strengthening contribution of Mn-bearing dispersoids. When the annealing temperature increased to 300°C, the YS reached 233 MPa for L-Mg alloy and 253 MPa for H-Mg alloy. Meanwhile, the YS increment between two homogenization conditions increased to 54 MPa in L-Mg and 42 MPa in H-Mg, indicating the superior recrystallization resistance of both alloys relative to the HTH. For these large differences, apart from the contribution of Mn-bearing dispersoids, and the recrystallization degree plays an important role.

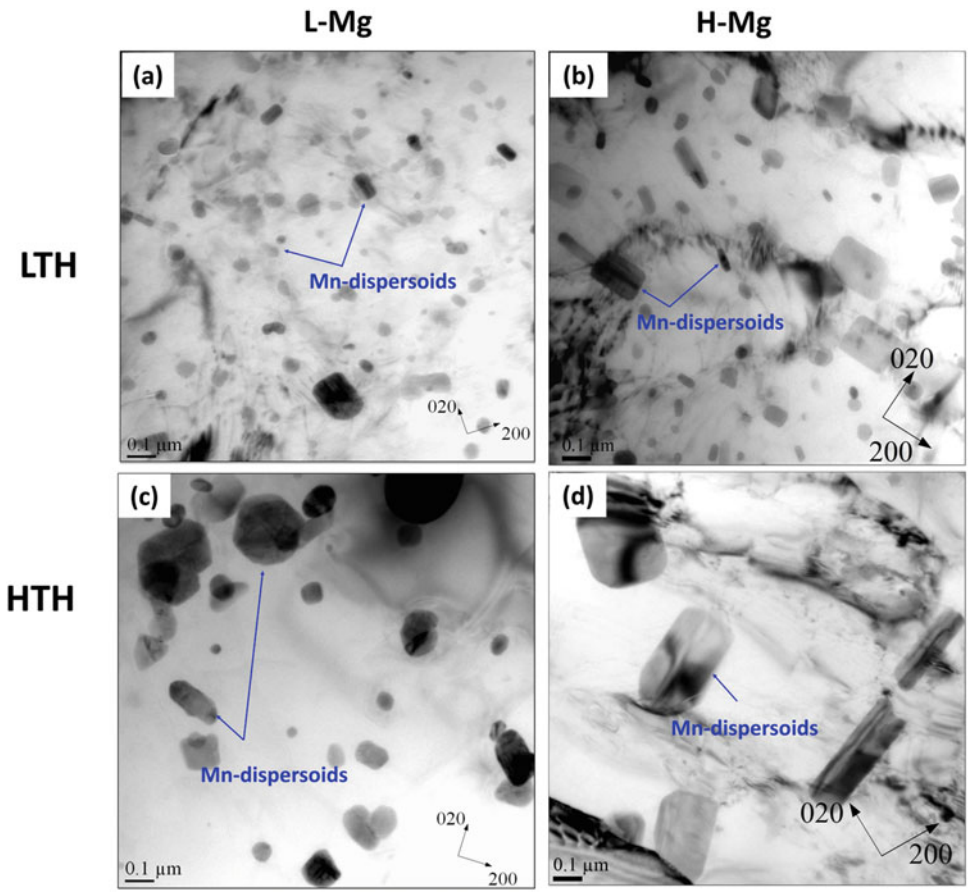

Fig. 4 Bright-field TEM images showing the distribution of Mn-bearing dispersoids after hot rolling: (**a**, **c**) L-Mg and (**b**, **d**) H-Mg alloys

Figure 4 displays bright-field TEM micrographs of the distribution of Mn-bearing dispersoids in two alloys after hot rolling. Compared to the dispersoids before rolling (Fig. 2c, d), the dispersoids become larger and less dense, owing to the high hot rolling temperature (500 °C) and interaction with dislocations during hot rolling [19]. It seems that such number density of dispersoids (343×10^{19} m^{-3} in L-Mg and 232×10^{19} m^{-3} in H-Mg) were still enough to retard the recrystallization during annealing. In addition, the samples homogenized at the low temperature always exhibited a notably higher number density of finer dispersoids than the samples homogenized at high temperature.

Figure 5 shows all Euler orientation maps, revealing the grain structure after 300 °C/1 h annealing. Both alloys (L-Mg and H-Mg) with the LTH (Fig. 5a, c) displayed a mixture of deformed structure and recrystallized structures. L-Mg alloys showed a lower recrystallization fraction of 55.4% compared to that containing in H-Mg alloy (58.9%), owing to the higher number density of fine dispersoids in L-Mg alloys. In addition, both alloys exhibited a significantly high fraction of low angle boundaries (i.e., 47.8% in L-Mg vs. 30.2% in H-Mg). On the other hand, the samples with the HTH reached a fully recrystallized structure (Fig. 5b, d). On comparison, the samples with the LTH exhibited a significantly higher fraction of low angle boundaries (i.e., 47.8% vs. 5.6% in L-Mg and 30.2% vs. 4.3% in H-Mg) than those with the HTH. The superior recrystallization resistance of both alloys with the LTH could be explained by the higher number density of thermally stable dispersoids (Fig. 4), providing higher Zener pinning effect on the dislocation, sub-grain boundaries migration. and hence improving the recrystallization resistance [4, 11, 13]. These results can further explain the significant difference in the YS between two homogenization conditions and between two alloys after annealing at 300–400 °C (Fig. 3). The present study found that Mg is involved in regulating the type and number density of Mn-bearing dispersoids. Furthermore, applying the low-temperature homogenization resulted in refining dispersoids, and hence improving mechanical properties and recrystallization resistance in a non-heat-treatable Al-Mg-Mn rolled alloy.

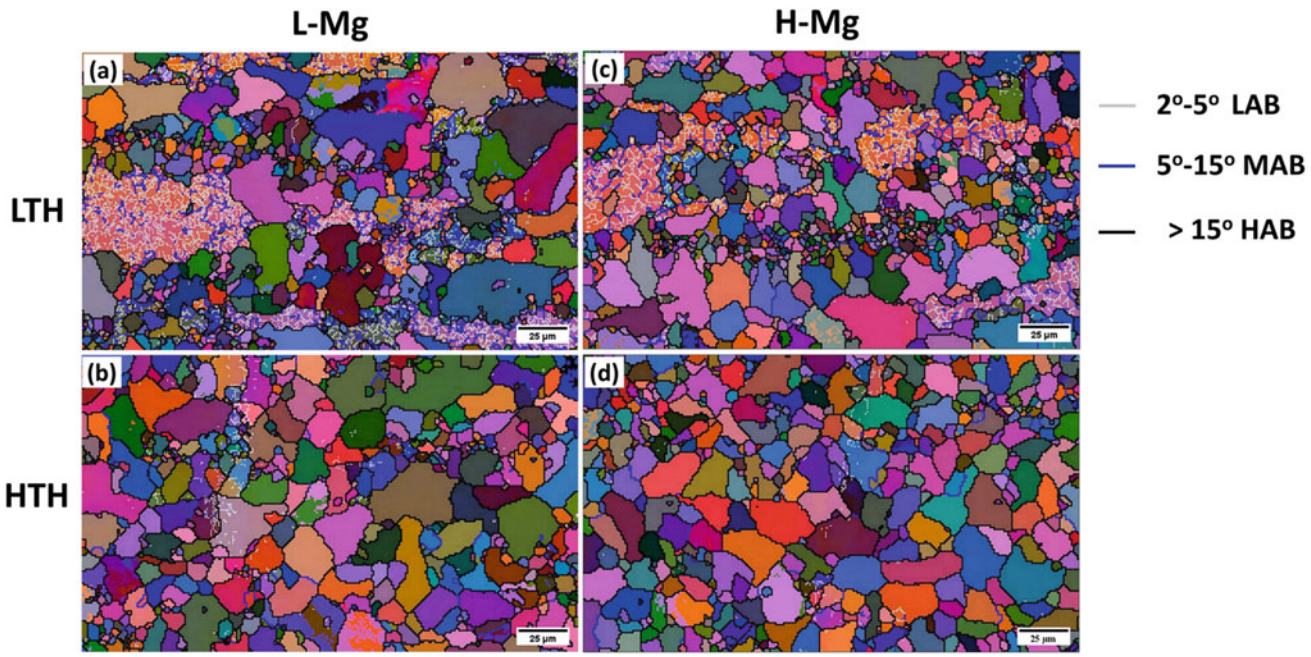

Fig. 5 All Euler orientation maps of the samples after cold rolling and annealing at 300 °C/1 h: (**a**, **b**) L-Mg and (**c**, **d**) H-Mg alloys

4 Conclusions

The present study investigated the formation of Mn-bearing dispersoids in two cold-rolled Al-Mg-Mn 5xxx alloys with high and low Mg levels as well as their impact on mechanical properties and recrystallization resistance. Finally, the following conclusions could be drawn.

1. During the low-temperature homogenization, a large number of Mn-bearing dispersoids precipitated in the dendrite cell interiors. The type, size, and number densities of dispersoids were strongly related to the Mg content. L-Mg alloy showed two types of fine Al_6Mn and α-Al(Mn,Fe)Si dispersoids, while the types of dispersoids changed to Al_4Mn and Al_6Mn by increasing the Mg level in H-Mg alloy.
2. The yield strength after cold rolling and 300 °C annealing reached 233 MPa for L-Mg and 253 MPa for H-Mg alloys homogenized at low temperature (LTH), respectively, showing an improvement of 30% and 20% over the high-temperature homogenization (HTH), and indicating the important effect of thermally stable Mn-bearing dispersoids.
3. Fine and densely distributed Mn-bearing dispersoids generated during low-temperature homogenization in both alloys could effectively hinder the dislocation and sub-grain boundary migration, and hence improve the recrystallization resistance of cold-rolled sheets. L-Mg alloy exhibited a better recrystallization resistance relative to H-Mg alloy.

Acknowledgements The authors would like to acknowledge the financial support of the Natural Sciences and Engineering Research Council of Canada (NSERC) under the Grant No. CRDPJ 514651-17 and Rio Tinto Aluminum through the Research Chair in the Metallurgy of Aluminum Transformation at the University of Quebec in Chicoutimi.

References

1. Davis JR (2001) Aluminum and aluminum alloys. ASM International, Materials Park, pp 66–66
2. Hirsch J (2011) Aluminium in innovative light-weight car design. Mater Trans 52(5):818–824. https://doi.org/10.2320/matertrans.L-MZ201132
3. Huskins E, Cao B, Ramesh K (2010) Strengthening mechanisms in an Al–Mg alloy. Mater Sci Eng A 527(6):1292–1298. https://doi.org/10.1016/j.msea.2009.11.056
4. Engler O, Kuhnke K, Hasenclever J (2017) Development of intermetallic particles during solidification and homogenization of two AA 5xxx series Al-Mg alloys with different Mg contents. J Alloys Compd 728:669–681. https://doi.org/10.1016/j.jallcom.2017.09.060

5. Algendy AY, Liu K, Chen XG (2021) Evolution of dispersoids during multistep heat treatments and their effect on rolling performance in an Al-5% Mg-0. 8% Mn alloy. Mater Charact 181:111487–111487. https://doi.org/10.1016/j.matchar.2021.111487
6. Liu K, Chen XG (2015) Development of Al-Mn-Mg 3004 alloy for applications at elevated temperature via dispersoid strengthening. Mater Des 84:340–350. https://doi.org/10.1016/j.matdes.2015.06.140
7. Algendy AY, Liu K, Rometsch P, Parson N, Chen XG (2022) Effects of AlMn dispersoids and Al_3(Sc, Zr) precipitates on the microstructure and ambient/elevated-temperature mechanical properties of hot-rolled AA5083 alloys. Mater Sci Eng A 855:143950. https://doi.org/10.1016/j.msea.2022.143950
8. Algendy AY, Liu K, Chen XG (2020) Formation of intermetallic phases during solidification in Al-Mg-Mn 5xxx alloys with various Mg levels MATEC web of conferences 326, France 02002-02002. https://doi.org/10.1051/matecconf/202032602002
9. Liu ZT, Wang C, Luo Q, You J, Zhou XL, Xu J, Mo YT, Song JW, Zha M, Wang HY (2020) Effects of Mg contents on the microstructure evolution and Fe–bearing phase selection of Al–Mg–Si–Fe alloys under sub–rapid solidification. Materialia 13:100850. https://doi.org/10.1016/j.mtla.2020.100850
10. Engler O, Liu Z, Kuhnke K (2013) Impact of homogenization on particles in the Al-Mg-Mn alloy AA 5454-Experiment and simulation. J Alloys Compd 560:111–122. https://doi.org/10.1016/j.jallcom.2013.01.163
11. Engler O, Miller-Jupp S (2016) Control of second-phase particles in the Al-Mg-Mn alloy AA 5083. J Alloys Compd 689:998–1010. https://doi.org/10.1016/j.jallcom.2016.08.070
12. Li Y, Zhang W, Marthinsen K (2012) Precipitation crystallography of plate-shaped Al_6(Mn, Fe) dispersoids in AA5182 alloy. Acta Mater 60(17):5963–5974. https://doi.org/10.1016/j.actamat.2012.06.022
13. Wang Y, Yang B, Gao M, Guan R (2022) Deformation behavior and dynamic recrystallization during hot compression in homogenized Al–6Mg–0.8 Mn alloys. Mater Sci Eng A 840:142953. https://doi.org/10.1016/j.msea.2022.142953
14. Huang H, Jiang F, Zhou J, Wei L, Zhong M, Liu X (2015) Hot deformation behavior and microstructural evolution of as-homogenized Al–6Mg–0.4 Mn–0.25 Sc–0.1 Zr alloy during compression at elevated temperature. J Alloys Compd 644:862–872. https://doi.org/10.1016/j.jallcom.2015.05.048
15. Li YJ, Arnberg L (2004) A eutectoid phase transformation for the primary intermetallic particle from Alm(Fe,Mn) to Al3(Fe,Mn) in AA5182 alloy. Acta Mater 52(10):2945–2952. https://doi.org/10.1016/j.actamat.2004.02.041
16. Liu Y, Luo L, Han C, Ou L, Wang J, Liu C (2016) Effect of Fe, Si and cooling rate on the formation of Fe- and Mn-rich Intermetallics in Al – 5Mg – 0. 8Mn alloy. J Mater Sci Technol 32(4):305–312. https://doi.org/10.1016/j.jmst.2015.10.010
17. Fang X, He G, Ruiz M, Zheng C, Wang Y, Li Z, Zhu Y (2019) Influence of annealing parameters on the mechanical properties of heterogeneous lamella structured 5083 aluminum alloy. Lett Mater 9(4s):556–560. https://doi.org/10.22226/2410-3535-2019-4-556-560
18. Wu JX, Gao C, Huang RY, Liu ZS, Zhao PZ (2018) Effect of cold deformation and annealing on microstructure and mechanical properties of 5083 aluminum alloy sheets. Mater Sci Forum Trans Tech Publ 913:49–54. https://doi.org/10.4028/www.scientific.net/MSF.913.49
19. Cabibbo M, Evangelista E, Vedani M (2005) Influence of severe plastic deformations on secondary phase precipitation in a 6082 Al-Mg-Si alloy. Metall Mater Trans A 36(5):1353–1364. https://doi.org/10.1007/s11661-005-0226-9